HHS Public Access

Author manuscript

Neuroimage. Author manuscript; available in PMC 2022 June 01.

Published in final edited form as:

Neuroimage. 2022 June ; 253: 119097. doi:10.1016/j.neuroimage.2022.119097.

A 4D infant brain volumetric atlas based on the UNC/UMN baby connectome project (BCP) cohort

Liangjun Chen[*], **Zhengwang Wu**, **Dan Hu**, **Ya Wang**, **Fenqiang Zhao**, **Tao Zhong**, **Weili Lin**, **Li Wang**, **Gang Li**[*]

Department of Radiology and BRIC, University of North Carolina at Chapel Hill, Chapel Hill, USA and for UNC/UMN Baby Connectome Project Consortium

Abstract

Spatiotemporal (four-dimensional) infant-dedicated brain atlases are essential for neuroimaging analysis of early dynamic brain development. However, due to the substantial technical challenges in the acquisition and processing of infant brain MR images, 4D atlases densely covering the dynamic brain development during infancy are still scarce. Few existing ones generally have fuzzy tissue contrast and low spatiotemporal resolution, leading to degraded accuracy of atlas-based normalization and subsequent analyses. To address this issue, in this paper, we construct a 4D structural MRI atlas for infant brains based on the UNC/UMN Baby Connectome Project (BCP) dataset, which features a high spatial resolution, extensive age-range coverage, and densely sampled time points. Specifically, 542 longitudinal T1w and T2w scans from 240 typically developing infants up to 26-month of age were utilized for our atlas construction. To improve the co-registration accuracy of the infant brain images, which typically exhibit dynamic appearance with low tissue contrast, we employed the state-of-the-art registration method and leveraged our generated reliable brain tissue probability maps in addition to the intensity images to improve the alignment of individual images. To achieve consistent region labeling on both infant and adult brain images for facilitating region-based analysis across ages, we mapped the widely used Desikan cortical parcellation onto our atlas by following an age-decreasing mapping manner. Meanwhile, the typical subcortical structures were manually delineated to facilitate the studies related to the subcortex. Compared with the existing infant brain atlases, our 4D atlas has much higher spatiotemporal resolution and preserves more structural details, and thus can boost accuracy in neurodevelopmental analysis during infancy.

Keywords

Infant; Brain atlas; Early neurodevelopment; MRI

[*]Corresponding author: cljun1990@gmail.com (L. Chen), gang_li@med.unc.edu (G. Li).

Credit authorship contribution statement

Liangjun Chen: Methodology, Software, Validation, Formal analysis, Investigation, Data curation, Writing – original draft, Visualization. **Zhengwang Wu:** Methodology, Software, Investigation, Data curation, Writing – review & editing. **Dan Hu:** Writing – review & editing. **Ya Wang:** Writing – review & editing, Data curation. **Fenqiang Zhao:** Writing – review & editing. **Tao Zhong:** Writing – review & editing. **Weili Lin:** Resources, Funding acquisition. **Li Wang:** Methodology, Writing – review & editing, Resources, Funding acquisition. **Gang Li:** Conceptualization, Methodology, Investigation, Writing – review & editing, Resources, Supervision, Project administration, Funding acquisition.

1. Introduction

Brain atlases, containing the *prior* knowledge on neuroanatomy and brain function, are commonly used in neuroimaging analysis (Li et al., 2019). A population-average brain atlas, which is preferred to represent typical anatomical structures of the population and shows high cross-individual validity, usually includes the population-representative intensity image, the associated probability maps for each tissue, and parcellation maps delineating anatomical or functional regions. During the last decades, more and more subjects were employed for building atlases to cater substantial brain anatomical differences across subjects. Meanwhile, the advancements in the techniques of image acquisition and processing significantly improved the quality of brain atlases, which can more accurately represent the brain structure with sharper contrast and more details, thus playing a critical role in modern neuroimaging researches (Yeh et al., 2018).

However, most existing atlases are developed for adult brains, and they are thus not suitable for the neurodevelopmental analysis of the developing infant brain (Kazemi et al., 2007; Shi et al., 2011), due to remarkable differences in imaging appearance, brain size, and brain shape. Specifically, different from the relatively stable adult brains, the infant brains have dynamic imaging appearances and significant brain development in size, shape, and folding in region-specific manners during the first two postnatal years. For example, the total brain volume increases 101% and 15% in the first and second years, respectively (Knickmeyer et al., 2008). Similarly, the entire cortical surface area expands about 200% in the first two years (Li et al., 2013). Such complex, dynamic, and regionally-heterogeneous development process is especially important for the later brain structure, function, and cognitive outcomes (Li et al., 2014a; 2019; Scott et al., 2016; Uematsu et al., 2012). This indicates that we need different atlases for brains at different developmental stages. Therefore, spatiotemporal (4D) brain atlases are highly demanded in normalizing and analyzing infant brain development. However, the difficulties in acquiring and processing infant brain images make the construction of high-quality infant brain atlases a challenging task. Specifically, due to the ongoing tissue development and myelination process, the infant brain MR images typically have dynamic imaging appearances and low tissue contrast (Prastawa et al., 2005; Shi et al., 2014; Xue et al., 2007), especially for the 6-month-old brain (Li et al., 2019; Wang et al., 2018), which significantly degrade the registration performance when aligning individual images into the common space. Thus, it is highly desired to have a 4D infant brain atlas with densely sampled time points and high spatial resolution to characterize detailed, age-related anatomical patterns.

Few pioneering infant brain volumetric atlases have been constructed. (Shi et al., 2011) combined HAMMER registration methods (Shen and Davatzikos, 2002; Wu et al., 2010) with a group-wise registration strategy (Wu et al., 2012) to create spatiotemporal infant atlases at 3 time points, i.e., 1-month, 12-month, and 24-month from 95 infants. (Kuklisova-Murgasova et al., 2011) built probabilistic atlases from the segmentation maps of 153 neonates from 29 to 44 weeks gestational age (GA). (Oishi et al., 2011) hierarchically used affine and nonlinear registration methods to construct an infant brain atlas from 33 neonates between 37 and 53 weeks postmenstrual age (PMA). (Fonov et al., 2009) created

an atlas with age ranging from birth to 4.5 years based on the NIH pediatric database using a nonlinear unbiased registration framework. (Akiyama et al., 2013) proposed a typical 6-month-old infant atlas from 60 infants with chronological age between 177 and 230 days. (Zhang et al., 2016) proposed spatiotemporal atlas at every three months in the first postnatal year using longitudinal scans from 35 infants with age ranging from 1-month to 12-month. (Schuh et al., 2018) published spatiotemporal neonatal brain atlas based on the Developing Human Connectome Project (dHCP) dataset (Makropoulos et al., 2018), which involved 275 neonates from 35 to 44 weeks PMA. We briefly summarized the recently published infant brain atlases in Table 1. As can be seen from the table, the volumetric spatiotemporal infant atlases from birth to 2 years of age are still rarely available, and few existing ones were generated based on few participants, low spatial resolution, and sparse temporal points, leading to degraded accuracy of subsequent analyses.

In this paper, we propose to construct a 4D volumetric atlas using a total of 542 high-quality infant brain MR scans from 240 subjects acquired by a large longitudinal infant brain dataset, i.e., the UNC/UMN Baby Connectome Project (BCP) (Howell et al., 2019). Our atlas densely covers the dynamic brain development during the first two years with 17 time points (i.e., 0, 1, 2, 3, 4, 5, 6, 7, 8, 9, 10, 11, 12, 15, 18, 21, and 24 months) and comprises of four components: (1) the group-representative T1w and T2w images; (2) the tissue probability maps (TPMs) for each tissue type; (3) the tissue segmentation maps (TSMs); and (4) the popularly-used Desikan cortical parcellation map (Desikan et al., 2006) and manually delineated subcortical labels. To mitigate the potential bias introduced by the hard threshold age grouping, we applied a sliding-window strategy to consider the subjects from the neighboring ages at each time point. To improve the registration performance, we first applied the infant brain extraction and analysis toolbox (iBEAT V2.0 Cloud) (Wang et al., 2018) to segment each scan into three tissue types and manually checked the achieved TPMs. Then, both the high-quality TPMs and the fuzzy intensity images were combined to align all images into the common space using the symmetric group-wise normalization (SyGN) approach (Avants et al., 2010), which is widely used in brain atlases building for human (Alexander et al., 2017; Dong et al., 2019) and non-human primates (Love et al., 2016). To achieve consistent cortical region labeling in both infant and adult brain images, we mapped the widely used Desikan cortical parcellation map to each age-specific atlas and also manually delineated the typical subcortical structures. To the best of our knowledge, our 4D infant atlas encodes the largest number of high-quality infant brain MR images and achieves the densest temporal sampling.

The organization of the paper is as follows. The atlas construction is detailed in Section II. In Section III, we qualitatively and quantitatively evaluated the performance of the proposed atlas, and compared them with the state-of-the-art atlases. In Section IV, we highlighted the novelty and significance of our atlas and discussed future works. Finally, we concluded in Section V.

2. Materials and methods

The proposed framework for building the 4D infant brain volumetric atlas is shown in Fig. 1. First, all the images were preprocessed and segmented using an infant brain dedicated

toolbox iBEAT V2.0 Cloud (Wang et al., 2018) (http://www.ibeat.cloud/). Next, the achieved TPMs along with T1w and T2w images were further input into the SyGN atlas construction algorithm (Avants et al., 2010) to build the templates at each time point. Finally, the widely-used Desikan cortical parcellation map in FreeSurfer was mapped to all the templates, and the subcortical structures were also manually delineated. In total, 542 MRI scans from 240 term-born subjects (128 females and 112 males) up to 26 months of age were utilized for atlas construction. The number of subjects at each scan age and the longitudinal distribution of the scans are illustrated in Fig. 2 and Fig. 3, respectively.

2.1. Participants and image acquisition

All MR images used for constructing our infant brain atlas are from the public BCP dataset, and all participants were recruited from a broad community to ensure the sample approximates the racial/ethnic and socioeconomic diversity of the US census.

During the data collection procedures, the inclusion criteria for enrolling children are as follows: 1) born from 37 to 42 weeks GA, 2) at an appropriate birth weight matching to the GA, and 3) free of major pregnancy and delivery complication. Children with the following criteria were excluded: 1) being adopted, 2) having schizophrenia, autism, bipolar disorder, or intellectual disability, 3) having any medical or genetic conditions related to growth, development, or cognition, 4) having any MRI contraindication, 5) maternal alcohol or illicit drug use, placental abruption, maternal pre-eclampsia, and maternal HIV status during pregnancy. More details of enrolling inclusion and exclusion criteria can be found in (Howell et al., 2019).

BCP MR images were acquired on two 3T Siemens Prisma MRI scanners located at the Biomedical Research Imaging Center (BRIC) at the University of North Carolina at Chapel Hill (UNC site) and the Center for Magnetic Resonance Research (CMRR) at the University of Minnesota (UMN site), respectively. To mitigate the harmonization problem of data acquired at two sites, the model of scanners is the same, and both scanners use the same Siemens 32 channel head coils and imaging protocol. Meanwhile, two sites used the same criteria to recruit and enroll subjects and performed the same imaging procedures and quality control criteria (i.e., excessive motion, insufficient coverage, and ghosting (Howell et al., 2019)). All scans were acquired while the infants were naturally sleeping, and their heads were secured in a vacuum fixation device with ear protection. We used both T1w and T2w images, which were acquired to provide anatomical information regarding brain structural development, to build our atlas. All T1w and T2w images have undergone visual inspection for quality control. Both T1w and T2w images had a resolution of $0.8 \times 0.8 \times 0.8$ mm^3 and were acquired with 208 sagittal slices using the following parameters, respectively: TR/TE = 2400/2.24 *ms* and TR/TE = 3200/564 *ms*.

In total, at the time of performing atlas construction, there were 775 scans from 306 subjects acquired within the age range from birth to 26 months. All structural MR images were visually checked by the experts after the image acquisition to assess the excessive motion, insufficient coverage, and ghosting. After the quality control, there remained 674 scans.

2.2. Image preprocessing and tissue segmentation

All images were preprocessed using the infant brain extraction and analysis toolkit (iBEAT V2.0 Cloud) (Wang et al., 2018). Specifically, N3 bias field correction (Sled et al., 1998) was firstly performed on all images for intensity inhomogeneity correction. Then, an infant-dedicated learning-based method (Zhang et al., 2019) was used for skull-stripping. Subsequently, for each subject, the T2w image was rigidly aligned onto the corresponding T1w image using FLIRT in FSL (Jenkinson et al., 2012). In addition, the FLIRT-based rigid registration was performed on all the BCP MR images to align them to the corresponding age-specific NIHPD atlas (Fonov et al., 2009) to normalize the brain orientation and posture, which benefits the later diffeomorphic non-linear image registration-based atlas building. As the NIHPD atlas sits in the MNI space, which is a commonly used space in neuroimaging studies, after the rigid alignment with the NIHPD atlas, the BCP MR images are also roughly aligned to the MNI space.

Due to the low tissue contrast in infant brain MR images, it is difficult to accurately align the subjects merely using the low contrast intensity images (i.e., T1w and T2w images). Therefore, we attempted to exploit the TPMs, including white matter (WM), gray matter (GM), and cerebrospinal fluid (CSF), in addition to the noisy intensity images to enhance the atlas construction with improved registration accuracy. The TPMs were obtained using our infant brain dedicated segmentation algorithm (Wang et al., 2018) in iBEAT V2.0 Cloud and further quality-controlled by expert. And 622 out of 674 scans survived in the quality control, in which only 542 scans had both T1w and T2w images. To build our atlas with as many as possible scans, such 542 scans up to 26 months of age were used to construct our 4D infant atlas.

2.3. Construction of infant brain atlas

2.3.1. Interval of the spatiotemporal atlas—During the first postnatal year, the infant brain exhibits more dynamic development, compared to the development within the second year (Knickmeyer et al., 2008). Therefore, to better characterize the dramatic neurodevelopment and capture more age-related anatomical patterns, 4D atlases with fine temporal granularity are highly necessary. However, the small temporal interval leads to a limited amount of data within each age group, which may adversely affect the quality of each age-specific atlas. Thus, we first monthly constructed age-dependent average atlases based on the images ranging from 0-month to 12-month. During the second postnatal year, the development of the infant brain is relatively sluggish, and the anatomical appearance of the infant brain is more similar to the adult brain. Hence, for the images from 13 to 26 months, we constructed the age-dependent average atlases every three months, i.e., 15-month, 18-month, 21-month, and 24-month. In sum, we totally built 17 age-specific atlases during the first two postnatal years.

As the infant brain develops rapidly, using the hard age-group strategy, for example, 90 days of age belonging to 3-month but 91 days of age belonging to 4-month, is inappropriate. Therefore, a sliding window strategy was applied to include scans from the neighboring time points to build each age-specific atlas, thus mitigating the issue introduced by the hard age threshold. Specifically, due to the rapid brain development, the width of the sliding

window should be small for building the atlases within the first year. Thus, we performed a fixed sliding window size of 3 months to build the atlases from 0-month to 12-month. For example, for the 1-month atlas construction, all scans at 0-month, 1-month, and 2-month were used. Of note, only the 0-month and 1-month scans were used to build the 0-month atlas. Similarly, a fixed sliding window size of 5 months was applied in building the atlases in the second year to account for the relatively sluggish anatomical changes of the infant brain during the second postnatal year. For example, we collected the scans from 13-month to 17-month to build the 15-month atlases. Such window sizes are determined according to our previous research experiences on infant brain tissue segmentation and analysis. By doing so, we can include as many as possible images for building each age-specific atlas, while still capturing the age-specific neurodevelopmental patterns.

2.3.2. Atlas building—Both the multi-modal intensity images and corresponding TPMs were adopted to align different subjects into the common space for boosting the registration accuracy. To achieve the atlas with unbiased shape and appearance, we used the symmetric group-wise normalization (SyGN) approach (Avants et al., 2010) provided in the ANTs toolkit (Avants and Gee, 2004; Avants et al., 2009), which is unbiased toward any specific individuals and does not require user input or *prior* information. Briefly, the SyGN approach (Fig. 4) consists of the following steps,

1. Build initial templates for T1w, T2w images, and TPMs, e.g., the TPMs of WM, GM, and CSF, by averaging the individual intensity images and TPMs.
2. Pair-wisely align each individual T1w, T2w images, and TPMs to the corresponding initial mean templates using the symmetric normalization (SyN) algorithm (Avants et al., 2008).
3. Average the warped individual T1w, T2w images, and TPMs, obtained during Step 2, to achieve updated template T1w, T2w images, and TPMs as appearance update.
4. Average the affine matrices and the deformation fields obtained during Step 2, and then apply the averaged affine matrices and deformation fields to each updated template achieved during Step 3, to optimize the shape of each template.
5. Use the updated templates obtained at Step 4 as the new initial templates in Step 2 for the next iteration until convergence.

Of note, in Step 2 at each iteration, the alignment transformation includes the rigid, affine, and non-rigid diffeomorphic registration. The greedy B-spline was chosen as the transformation model, and cross-correlation was the similarity metric for the brain registration, with default shrinkage factors, smoothing factors, and max iterations of 8×4×2×1, 3×2×1×0, and 100×70×50×10, respectively. Once the algorithm converged, the TPMs of atlases at each time point were utilized to build the TSMs.

2.4. Parcellation maps

In many applications, the gray matter of the brain is partitioned into meaningful anatomical regions of interest (ROIs), with each region corresponding to a unique label. These ROIs

are generally used for comparison or quantification of the region-based features (Douaud et al., 2006; Etzel et al., 2009; Frost and Goebel, 2013; Good et al., 2002). In our atlas, we warped the widely used FreeSurfer Desikan adult cortical parcellation map (Desikan et al., 2006), which was proposed based the sulcal-gyral geometric information of primary cortical folds, onto our atlas to facilitate the ROI-based longitudinal analysis across the lifespan, e.g., the neonates, infants, toddlers, preschoolers, old children, adolescents, and adults, in a consistent manner. Although, directly using adult parcellation may introduce minor bias for the baby brains due to the differences between infant and adult brain, based on the previous study, the major and secondary cortical folding has been established at the term birth (Duan et al., 2020; Hill et al., 2010; Li et al., 2014b; 2019), making it suitable to propagate the Desikan parcellation onto our atlas. To this end, first, we reconstructed the cortical surfaces of each template (Li et al., 2014a) and mapped them onto a sphere for accurate cortical registration. Second, we propagated the Desikan parcellation map to the reconstructed cortical surfaces of 24-month atlas using the cortical surface registration method (Yeo et al., 2009) for aligning cortical folds. Third, we propagated the cortical surface-based 24-month parcellation map onto each other age-specific atlas by following an age-decreasing manner. Finally, the warped parcellation maps on the reconstructed cortical surfaces were projected back to the image atlas space.

For the subcortical gray matter, an expert manually labeled 12 subcortical structures, i.e., bilateral thalamus, caudate, putamen, pallidum, hippocampus, and amygdala on 0-month, 3-month, 6-month, 9-month, 12-month, 15-month, 18-month, and 24-month atlases. Subsequently, we transformed the subcortical segmentation maps to the neighbor atlases by performing SyN-based registration, and further manually corrected these warped subcortical label maps to achieve the final subcortical labels. Therefore, the parcellations maps of each proposed atlas include total 82 structures (35 cortical ROIs and 6 subcortical ROIs in each hemisphere), shown in Fig. 5.

3. Results

3.1. Overview of the proposed 4D infant atlas

We present our atlas in Fig. 6. From left to right shows the T1w and T2w templates, TPMs of GM, WM, CSF, and TSMs. The scan number n used for building each age-specific atlas is also shown in Fig. 6. As the individual scans have been all rigidly aligned to the NIHPD atlas, which sits in the MNI space, the proposed atlas was also built in the MNI space with a size of $243 \times 291 \times 198$ and resolution of $0.8 \times 0.8 \times 0.8\ mm^3$. It is worth noting that this atlas shows the dynamic development of infant brain in shape, size, appearances, and anatomical structures, especially during the first year. Each voxel in the TPMs contains a value between 0 and 1, describing the average likelihood that the voxel belongs to a specific tissue type, i.e., GM, WM, and CSF.

3.2. The comparison of the proposed infant atlas and state-of-the-art infant atlases on BCP dataset

To evaluate the performance of the proposed 4D infant atlas, we further included four state-of-the-art infant atlases for both qualitative and quantitative comparisons. The first

comparison atlas is a neonate atlas created by (Schuh et al., 2018), which is derived from the developing human connectome project (dHCP) dataset with a high resolution of 0.5 × 0.5 × 0. 5 mm^3, using MR images from 275 neonates with age ranging between 35 and 44 weeks in postmenstrual age. We included the atlas at 44 weeks as the state-of-the-art atlas of neonates and compared it with the 1-month atlas proposed in this study. The second comparison atlas includes templates at 1-month, 12-month, and 24-month, which is proposed by (Shi et al., 2011) using scans from 95 neonates and has a resolution of 1 × 1 × 1 mm^3. The third atlas is a spatiotemporal longitudinal infant atlas (Zhang et al., 2016) with age ranging from birth to 12 months, which includes templates for time points at 1-month, 3-month, 6-month, 9-month, and 12-month. This atlas is constructed using 150 longitudinal scans from 35 healthy infants and has a resolution of 1 × 1 × 1 mm^3. The fourth one is the infant atlas proposed by (Fonov et al., 2009) using 317 scans from 108 children with a resolution of 1 × 1 × 1 mm^3 and age ranging from birth to 54 months.

3.2.1. Qualitative comparison—In this subsection, we visually compared the proposed 4D atlas with the aforementioned available atlases. The typical image slices of the proposed T1w and T2w templates and the corresponding atlases are illustrated in Fig. 7.

For neonates, we can find that our atlas shows more clear structures in both T1w and T2w templates, which are comparable with the neonate-dedicated atlas proposed by (Schuh et al., 2018). Meanwhile, for other age groups, it can be observed that the proposed atlas shows the most structural details. In particular, we can see clear structures with distinct boundaries in the cortical regions shown by close-up views. Note that successfully preserving the cortical structures of the infant brain is critical for many related typical applications, e.g., spatial normalization and tissue segmentation.

3.2.2. Quantitative comparison—To quantitatively compare the performance of the proposed atlas, we performed the atlas-based tissue segmentation using the proposed atlas and representative atlases. Specifically, we randomly selected 54 scans from 542 scans (10% scans at each age group) as the test scans and built the T1w and T2w templates based on the remaining 488 scans using the same strategies detailed in Section II. Then, we registered each atlas to each test image using the T1w image, and warped the TSMs provided by each atlas to the individuals using the obtained deformation fields. We still used ANTs to perform the registration between the test images and atlases. We used the following default parameters of æantsRegistrationSyN.shg: transform type = s, radius for cross-correlation metric = 4, and spline distance for deformable B-spline SyN transform = 26.

We used the Dice ratio (mean and standard deviation) (Dice, 1945) to measure the overlap between the individual TSMs warped from each atlas and the manually-corrected TSMs of test images, which were provided in the BCP dataset and served as the ground-truth. For the source segmentation label S and target segmentation label T, the Dice ratio is defined as $Dice = 2|S \cap T|/(|S| + |T|)$. The higher values of the Dice ratio indicate the better agreements between two segmentation labels.

The values of the Dice ratio of 54 test scans between the atlas-based segmentation maps and the manually-corrected segmentation maps are presented in Table 2 and the paired

t-test was conducted. For neonates, the proposed atlas performed comparably with the neonate-dedicated dHCP atlas ($p > 0.05$) and is significantly better than the infant atlases proposed by (Shi et al., 2011) and (Zhang et al., 2016) in segmenting all types of tissues ($p < 0.01$). For other age groups, the segmentation based on the proposed atlas achieves the highest values of Dice ratio compared to the ones obtained by other atlases ($p < 0.05$).

To better evaluate our atlas, in addition to the group-average Dice ratio values, we use the violin plots (Fig. 8) to depict the distribution of the individual Dice ratio values obtained by the atlas in (Zhang et al., 2016) and our atlas. As (Zhang et al., 2016) only includes the age-specific atlases within the first year of life, we selected the testing scans within the first year for fair comparisons. From Fig. 8, we observe that our atlas achieved improved segmentation accuracy for each tissue type ($p < 0.0001$), compared to the state-of-the-art infant atlas (Zhang et al., 2016). To better reflect the paired nature of the test images, we pair-wisely connected the Dice ratio values based on different atlases.

Overall, these results demonstrate that the registration based on the proposed atlas yields a comparable or higher quality than that based on the competing atlases, which is beneficial for the atlas-based segmentation and other subsequent statistical analyses.

3.3. Significance of tissue probability maps in infant atlas construction

As mentioned before, the quality of infant brain MR image registration is severely limited by insufficient spatial resolution, low tissue contrast, and dynamic intensity changes. Therefore, we jointly used the intensity images and TPMs to build our atlases, and qualitatively and quantitatively compared them with the atlases constructed by both T1w and T2w images in this section.

3.3.1. Qualitative comparison—The typical slices of the constructed T1w and T2w templates are shown in Fig. 9. We can easily observe that, compared to the templates created based on intensity images, the templates built based on both intensity images and the TPMs show more cortical structural details, especially in the regions marked by the boxes. Therefore, these results proved that leveraging both the intensity images and the TPMs can help significantly enhance the accuracy of registration, and consequently build higher-quality atlas, which preserves more details of the age-specific appearance and anatomical structures during infancy.

3.3.2. Quantitative comparison—We used the same 54 randomly selected images as the test images to compare the quality of atlas built w/o the TPMs. Similarly, we registered the atlas built with only the intensity images to each test image and then warped the TSMs to the test images, so as to obtain the TSMs for each test image, and further compared them with the segmentations obtained by atlas built with both the intensity images and the TPMs in terms of Dice ratio.

The values of the Dice ratio on intensity image-based atlas at each age point are summarized in Table 3. It is obvious that the intensity image-based atlas achieved a lower Dice ratio than the atlas built with both the intensity images and the TPMs ($p < .05$). This is attributed to

the superior registration accuracy, and thus quantitatively verifies the effectiveness of using TPMs to help improve the quality of the infant brain atlas.

3.4. Comparison of the proposed infant atlas and state-of-the-art infant atlases on an unseen dataset

To further certify the effectiveness of the proposed atlas on images acquired using different scanners with different protocols, we adopted a new infant brain MRI dataset from the National Database of Autism Research (NDAR) (Payakachat et al., 2016). The MR images were scanned using Siemens Magnetom TrioTim 3T scanners, and T1w images were acquired with 160 sagittal slices using parameters: TR/TE=2400/3.16 *ms* and resolution = $1 \times 1 \times 1$ mm^3, which are totally different from the proposed atlas and other competing atlases. This dataset has a total of 980 scans, which are scanned at 6-month, 12-month, and 24-month of age, respectively. In this section, we compared the proposed atlas with the atlases proposed by (Shi et al., 2011) and (Zhang et al., 2016) by performing an image normalization task. Specifically, 300 MR images (100 images from each time point) were randomly selected and registered onto each atlas using ANTs. Then the corresponding TSMs were warped onto the atlases. The Dice ratio value between every two warped individual TSMs at each age was calculated to demonstrate the better performance of the proposed atlas in normalizing individual images. The results of the Dice ratio are presented in Table 4.

From Table 4, we can clearly find that the images warped onto the proposed atlas achieved higher Dice ratio values, especially for the 6-month images (with the lowest contrast due to the myelination process), compared to other state-of-the-art infant brain atlases, demonstrating the superior normalization accuracy achieved by the proposed 4D atlas (paired t-test $p < 0.01$). Consequently, the high normalization accuracy inversely verifies the high-quality of the proposed atlas, making it a valuable tool for the studies of early brain development.

4. Discussion

Many previous studies have proved that applying adult-based atlases as a reference to normalize MR images of infant brains is less accurate than using infant-dedicated atlases (Fillmore et al., 2015; Fonov et al., 2011; Sanchez et al., 2012). However, the infant-dedicated 4D brain atlases, which reflect the dynamic and regionally-heterogeneous complex neurodevelopment, are still poorly studied, and few existing ones generally have low tissue contrast and fuzzy anatomical structures (Fonov et al., 2009; Shi et al., 2011; Zhang et al., 2016). Therefore, in this work, we mainly aim to build high-quality and publicly available 4D infant brain MRI atlas with clear and sharp structural patterns.

Our atlas was constructed for subjects with a specific age ranging from birth to 26-month using 542 MRI scans from 240 subjects. To the best of our knowledge, it is the largest dataset with the highest spatial resolution for constructing infant atlas so far. Considering that volumetric image registration accuracy can be significantly improved by an age-matching template (Shen et al., 2007), we built the 4D atlas every month within the first year and every three months within the second year. Meanwhile, we applied a sliding window strategy to further mitigate the potential bias caused by the hard-thresholded age

grouping strategy. Thus, as proved in (Kazemi et al., 2007), based on our temporally-dense spatiotemporal atlas, an atlas with the most appropriate age can be applied to various applications to help obtain more accurate results. Nevertheless, many other factors may still influence the quality of the atlas, such as the MRI data quality and registration techniques. In this work, all the MR images are from the BCP dataset, which is acquired in a high spatial resolution of $0.8 \times 0.8 \times 0.8\ mm^3$ with infant dedicated protocol and techniques. In addition, the accuracy of registration for the infant brain MR images is significantly degraded due to the low image contrast and appearance changes, which are caused by the underlying spatiotemporally-nonuniform myelination process during early brain development. Hence, to enhance the registration quality, we jointly used the intensity images and high-quality TPMs to perform the atlas construction and consequently achieved atlas that preserves notably increased details. Meanwhile, to ensure the quality of the atlas, we applied the state-of-the-art SyGN template construction technique (Avants et al., 2010) to build each age-specific atlas. Finally, the cortical parcellation map used in FreeSurfer, which is routinely applied in neuroimaging studies, was carefully mapped to each atlas and combined with manually-delineated subcortical segmentation maps for region-based infant brain studies, e.g., volumetric measurement and functional connectivity.

As illustrated in the experiments, the proposed atlas not only encompasses obviously increased structural details and sharper tissue contrast, but also outperforms the state-of-the-art infant atlases in both segmentation and normalization tasks. Therefore, our 4D volumetric infant brain atlas has plenty of applications in neuroimaging studies: 1) our atlas can serve as a template to provide *priori* knowledge for the teaching of infant brain anatomy and function; 2) our atlas can be applied to normalize different MR images into a unified common space to investigate the group-level developmental patterns of the infant brain to advance our understanding of the dynamic development on both normal and abnormal brains during infancy; 3) our atlas is highly useful in atlas-based tissue segmentation and brain parcellation for studying infant brain structural and functional network development. Meanwhile, it also helps generate precise initial results of tissue segmentation and brain parcellation for deep learning-based methods; 4) computational results and discoveries from different studies can be visualized, reported, and reposited in our atlases, thus allowing direct comparisons across infant studies.

However, it is worth noting that, compared to the cortical surface atlas, the volumetric atlas may not be the best choice for aligning the cortical folds, which typically have complex shapes in geometry. Therefore, it is more suitable to use cortical surface atlas for the normalization of cortical folds, since it respects the geometry and topology of the highly convoluted cerebral cortex and thus can lead to improved accuracy for the cortex (Coalson et al., 2018; Li et al., 2015). The proposed volumetric atlas is more suitable for conducting the volumetric-based analysis and normalizing the subcortical regions, but still achieves reasonable accuracy for cortical registration, to promote the understanding of early postnatal brain neurodevelopment.

Additionally, the influence of the age difference within each age group is not considered in current work and can be potentially addressed by the conventional kernel regression method. However, since the infant brain has regionally-heterogeneous and large nonlinear

development and the performance of this regression method is sensitive to the kernel size, it is very challenging to choose an appropriate kernel size to fit such complex development. Inspired by the great success of deep convolutional neural networks, especially conditional generative adversarial networks (Michelsanti and Tan, 2017), proposing an advanced multi-input deep architecture to simultaneously consider the input images and age to generate age-specific atlas should be very interesting as our future work. Meanwhile, inspired by the recently proposed surface-guided learning-based image registration method (Dalca et al., 2019), integration of the surface-based registration into such deep network architecture to help enhance the registration accuracy in building high-quality infant atlases with sharper anatomical boundaries would also be a potential promising direction. Finally, in this work, we propagate the Desikan adult cortical parcellation onto our atlas to facilitate the ROI-based lifespan studies. However, an infant dedicated parcellation strategy is highly desired to more precisely delineate the neuroanatomical structures of the infant brain (Oishi et al., 2019; Wang et al., 2019), which will be one of our future works as well. Moreover, we will also propagate other widely-used parcellation maps, i.e., AAL parcellation (Tzourio-Mazoyer et al., 2002), onto our atlas to further promote different ROI-based studies and expand the application areas of our atlas.

5. Conclusion

In this paper, we propose a dense volumetric spatiotemporal infant MRI atlas with age ranging from birth to 24-month. Our atlas was built based on 542 high-quality scans from 240 healthy infant subjects acquired in the UNC/UMN Baby Connectome Project (BCP). To cope with the dynamic and regionally-heterogeneous image contrast and appearance changes in infant brain MR images, an infant brain dedicated pipeline was performed for prepossessing and tissue segmentation. Then both the T1w, T2w images, and the tissue probability maps were combined with the state-of-the-art group-wise atlas construction technique to increase the accuracy of registration and ensure the high-quality of the proposed atlas. Moreover, the widely used Desikan cortical parcellation map was carefully mapped to each atlas, and 12 subcortical structures are manually delineated and included in the cortical parcellation maps. The experimental results indicate that our 4D atlas has markedly improved clarity with more abundant structural details and has superior performance in atlas-based segmentation and normalization, especially for the age groups with dramatic myelination process, compared with other state-of-the-art infant brain atlases. Therefore, our 4D atlas is a good choice for studying early brain growth patterns and other clinical applications, which will be publicly available on NITRC (https://www.nitrc.org/projects/uncbcp_4d_atlas/) website to remarkably facilitate the studies on early human brain development.

Acknowledgment

This work was partially supported by NIH grants (MH116225, MH117943, MH109773, and MH123202). This work also utilizes approaches developed by an NIH grant (1U01MH110274) and the efforts of the UNC/UMN Baby Connectome Project Consortium.

The NDAR dataset used in this manuscript were obtained from the NIH supported National Database for Autism Research (NDAR), which is a collaborative informatics system created by the National Institutes of Health to provide a national resource to support and accelerate research in autism. This manuscript reflects the views of

the authors and may not reflect the opinions or views of the NIH or of the Submitters submitting original data to NDAR.

References

Akiyama LF, Richards TR, Imada T, Dager SR, Wroblewski L, Kuhl PK, 2013. Age-specific average head template for typically developing 6-month-old infants. PLoS ONE 8 (9), e73821. [PubMed: 24069234]

Alexander B, Murray AL, Loh WY, Matthews LG, Adamson C, Beare R, Chen J, Kelly CE, Rees S, Warfield SK, et al. , 2017. A new neonatal cortical and subcortical brain atlas: the melbourne children's regional infant brain (m-crib) atlas. Neuroimage 147, 841–851. [PubMed: 27725314]

Avants B, Gee JC, 2004. Geodesic estimation for large deformation anatomical shape averaging and interpolation. Neuroimage 23, S139–S150. [PubMed: 15501083]

Avants BB, Epstein CL, Grossman M, Gee JC, 2008. Symmetric diffeomorphic image registration with cross-correlation: evaluating automated labeling of elderly and neurodegenerative brain. Med Image Anal 12 (1), 26–41. [PubMed: 17659998]

Avants BB, Tustison N, Song G, 2009. Advanced normalization tools (ants). Insight j 2, 1–35.

Avants BB, Yushkevich P, Pluta J, Minkoff D, Korczykowski M, Detre J, Gee JC, 2010. The optimal template effect in hippocampus studies of diseased populations. Neuroimage 49 (3), 2457–2466. [PubMed: 19818860]

Coalson TS, Van Essen DC, Glasser MF, 2018. The impact of traditional neuroimaging methods on the spatial localization of cortical areas. Proceedings of the National Academy of Sciences 115 (27), E6356–E6365.

Dalca AV, Balakrishnan G, Guttag J, Sabuncu MR, 2019. Unsupervised learning of probabilistic diffeomorphic registration for images and surfaces. Med Image Anal 57, 226–236. [PubMed: 31351389]

Desikan RS, Ségonne F, Fischl B, Quinn BT, Dickerson BC, Blacker D, Buckner RL, Dale AM, Maguire RP, Hyman BT, et al. , 2006. An automated labeling system for subdividing the human cerebral cortex on mri scans into gyral based regions of interest. Neuroimage 31 (3), 968–980. [PubMed: 16530430]

Dice LR, 1945. Measures of the amount of ecologic association between species. Ecology 26 (3), 297–302.

Dong H-M, Castellanos FX, Yang N, Zhang Z, He Y, Zhang L, Xu T, Holmes AJ, Yeo BT, Chen F, et al. , 2019. Generating templates and growth charts for school-aged brain development. bioRxiv 747352.

Douaud G, Gaura V, Ribeiro M-J, Lethimonnier F, Maroy R, Verny C, Krystkowiak P, Damier P, Bachoud-Levi A-C, Hantraye P, et al. , 2006. Distribution of grey matter atrophy in huntingtons disease patients: a combined roi-based and voxel-based morphometric study. Neuroimage 32 (4), 1562–1575. [PubMed: 16875847]

Duan D, Xia S, Rekik I, Wu Z, Wang L, Lin W, Gilmore JH, Shen D, Li G, 2020. Individual identification and individual variability analysis based on cortical folding features in developing infant singletons and twins. Hum Brain Mapp 41 (8), 1985–2003. [PubMed: 31930620]

Etzel JA, Gazzola V, Keysers C, 2009. An introduction to anatomical roi-based fmri classification analysis. Brain Res. 1282, 114–125. [PubMed: 19505449]

Fillmore PT, Phillips-Meek MC, Richards JE, 2015. Age-specific mri brain and head templates for healthy adults from 20 through 89 years of age. Front Aging Neurosci 7, 44. [PubMed: 25904864]

Fonov V, Evans AC, Botteron K, Almli CR, McKinstry RC, Collins DL, Group BDC, et al. , 2011. Unbiased average age-appropriate atlases for pediatric studies. Neuroimage 54 (1), 313–327. [PubMed: 20656036]

Fonov VS, Evans AC, McKinstry RC, Almli C, Collins D, 2009. Unbiased nonlinear average age-appropriate brain templates from birth to adulthood. Neuroimage (47) S102.

Frost MA, Goebel R, 2013. Functionally informed cortex based alignment: an integrated approach for whole-cortex macro-anatomical and roi-based functional alignment. Neuroimage 83, 1002–1010. [PubMed: 23899723]

Good CD, Scahill RI, Fox NC, Ashburner J, Friston KJ, Chan D, Crum WR, Rossor MN, Frackowiak RS, 2002. Automatic differentiation of anatomical patterns in the human brain: validation with studies of degenerative dementias. Neuroimage 17 (1), 29–46. [PubMed: 12482066]

Hill J, Dierker D, Neil J, Inder T, Knutsen A, Harwell J, Coalson T, Van Essen D, 2010. A surface-based analysis of hemispheric asymmetries and folding of cerebral cortex in term-born human infants. J. Neurosci 30 (6), 2268–2276. [PubMed: 20147553]

Howell BR, Styner MA, Gao W, Yap P-T, Wang L, Baluyot K, Yacoub E, Chen G, Potts T, Salzwedel A, et al. , 2019. The UNC/UMN baby connectome project (BCP): an overview of the study design and protocol development. Neuroimage 185, 891–905. [PubMed: 29578031]

Jenkinson M, Beckmann CF, Behrens TE, Woolrich MW, Smith SM, 2012. Fsl. Neuroimage 62 (2), 782–790. [PubMed: 21979382]

Kazemi K, Moghaddam HA, Grebe R, Gondry-Jouet C, Wallois F, 2007. A neonatal atlas template for spatial normalization of whole-brain magnetic resonance images of newborns: preliminary results. Neuroimage 37 (2), 463–473. [PubMed: 17560795]

Knickmeyer RC, Gouttard S, Kang C, Evans D, Wilber K, Smith JK, Hamer RM, Lin W, Gerig G, Gilmore JH, 2008. A structural mri study of human brain development from birth to 2 years. J. Neurosci 28 (47), 12176–12182. [PubMed: 19020011]

Kuklisova-Murgasova M, Aljabar P, Srinivasan L, Counsell SJ, Doria V, Serag A, Gousias IS, Boardman JP, Rutherford MA, Edwards AD, et al. , 2011. A dynamic 4d probabilistic atlas of the developing brain. Neuroimage 54 (4), 2750–2763. [PubMed: 20969966]

Li G, Nie J, Wang L, Shi F, Gilmore JH, Lin W, Shen D, 2014. Measuring the dynamic longitudinal cortex development in infants by reconstruction of temporally consistent cortical surfaces. Neuroimage 90, 266–279. [PubMed: 24374075]

Li G, Nie J, Wang L, Shi F, Lin W, Gilmore JH, Shen D, 2013. Mapping region-specific longitudinal cortical surface expansion from birth to 2 years of age. Cerebral cortex 23 (11), 2724–2733. [PubMed: 22923087]

Li G, Wang L, Shi F, Gilmore JH, Lin W, Shen D, 2015. Construction of 4d high--definition cortical surface atlases of infants: methods and applications. Med Image Anal 25 (1), 22–36. [PubMed: 25980388]

Li G, Wang L, Shi F, Lin W, Shen D, 2014. Simultaneous and consistent labeling of longitudinal dynamic developing cortical surfaces in infants. Med Image Anal 18 (8), 1274–1289. [PubMed: 25066749]

Li G, Wang L, Yap P-T, et al. , 2019. Computational neuroanatomy of baby brains: a review. Neuroimage 185, 906–925. [PubMed: 29574033]

Love SA, Marie D, Roth M, Lacoste R, Nazarian B, Bertello A, Coulon O, Anton J-L, Meguerditchian A, 2016. The average baboon brain: MRI templates and tissue probability maps from 89 individuals. Neuroimage 132, 526–533. [PubMed: 26975558]

Makropoulos A, Robinson EC, Schuh A, Wright R, Fitzgibbon S, Bozek J, Counsell SJ, Steinweg J, Vecchiato K, Passerat-Palmbach J, et al. , 2018. The developing human connectome project: a minimal processing pipeline for neonatal cortical surface reconstruction. Neuroimage 173, 88–112. [PubMed: 29409960]

Michelsanti D, Tan Z-H, 2017. Conditional generative adversarial networks for speech enhancement and noise-robust speaker verification. arXiv preprint arXiv:1709.01703.

Oishi K, Chang L, Huang H, 2019. Baby brain atlases. Neuroimage 185, 865–880. [PubMed: 29625234]

Oishi K, Mori S, Donohue PK, Ernst T, Anderson L, Buchthal S, Faria A, Jiang H, Li X, Miller MI, et al. , 2011. Multi-contrast human neonatal brain atlas: application to normal neonate development analysis. Neuroimage 56 (1), 8–20. [PubMed: 21276861]

Payakachat N, Tilford JM, Ungar WJ, 2016. National database for autism research (ndar): big data opportunities for health services research and health technology assessment. Pharmacoeconomics 34 (2), 127–138. [PubMed: 26446859]

Prastawa M, Gilmore JH, Lin W, Gerig G, 2005. Automatic segmentation of mr images of the developing newborn brain. Med Image Anal 9 (5), 457–466. [PubMed: 16019252]

Sanchez CE, Richards JE, Almli CR, 2012. Age-specific mri templates for pediatric neuroimaging. Dev Neuropsychol 37 (5), 379–399. [PubMed: 22799759]

Schuh A, Makropoulos A, Robinson EC, Cordero-Grande L, Hughes E, Hutter J, Price AN, Murgasova M, Teixeira RPA, Tusor N, et al. , 2018. Unbiased construction of a temporally consistent morphological atlas of neonatal brain development. bioRxiv 251512.

Scott JA, Grayson D, Fletcher E, Lee A, Bauman MD, Schumann CM, Buonocore MH, Amaral DG, 2016. Longitudinal analysis of the developing rhesus monkey brain using magnetic resonance imaging: birth to adulthood. Brain Structure and Function 221 (5), 2847–2871. [PubMed: 26159774]

Shen D, Davatzikos C, 2002. Hammer: hierarchical attribute matching mechanism for elastic registration. IEEE Trans Med Imaging 21 (11), 1421–1439. [PubMed: 12575879]

Shen S, Szameitat AJ, Sterr A, 2007. Vbm lesion detection depends on the normalization template: a study using simulated atrophy. Magn Reson Imaging 25 (10), 1385–1396. [PubMed: 17467945]

Shi F, Wang L, Wu G, Li G, Gilmore JH, Lin W, Shen D, 2014. Neonatal atlas construction using sparse representation. Hum Brain Mapp 35 (9), 4663–4677. [PubMed: 24638883]

Shi F, Yap P-T, Wu G, Jia H, Gilmore JH, Lin W, Shen D, 2011. Infant brain atlases from neonates to 1-and 2-year-olds. PLoS ONE 6 (4), e18746. [PubMed: 21533194]

Sled JG, Zijdenbos AP, Evans AC, 1998. A nonparametric method for automatic correction of intensity nonuniformity in mri data. IEEE Trans Med Imaging 17 (1), 87–97. [PubMed: 9617910]

Tzourio-Mazoyer N, Landeau B, Papathanassiou D, Crivello F, Etard O, Delcroix N, Mazoyer B, Joliot M, 2002. Automated anatomical labeling of activations in SPM using a macroscopic anatomical parcellation of the MNI MRI single-subject brain. Neuroimage 15 (1), 273–289. [PubMed: 11771995]

Uematsu A, Matsui M, Tanaka C, Takahashi T, Noguchi K, Suzuki M, Nishijo H, 2012. Developmental trajectories of amygdala and hippocampus from infancy to early adulthood in healthy individuals.

Wang F, Lian C, Wu Z, Zhang H, Li T, Meng Y, Wang L, Lin W, Shen D, Li G, 2019. Developmental topography of cortical thickness during infancy. Proceedings of the National Academy of Sciences 116 (32), 15855–15860.

Wang L, Li G, Shi F, Cao X, Lian C, Nie D, Liu M, Zhang H, Li G, Wu Z, et al., 2018. Volume-based analysis of 6-month-old infant brain MRI for autism biomarker identification and early diagnosis. In: MICCAI, pp. 411–419.

Wu G, Wang Q, Jia H, Shen D, 2012. Feature-based groupwise registration by hierarchical anatomical correspondence detection. Hum Brain Mapp 33 (2), 253–271. [PubMed: 21391266]

Wu G, Yap P-T, Kim M, Shen D, 2010. Tps-hammer: improving hammer registration algorithm by soft correspondence matching and thin-plate splines based deformation interpolation. Neuroimage 49 (3), 2225–2233. [PubMed: 19878724]

Xue H, Srinivasan L, Jiang S, Rutherford M, Edwards AD, Rueckert D, Hajnal JV, 2007. Automatic segmentation and reconstruction of the cortex from neonatal mri. Neuroimage 38 (3), 461–477. [PubMed: 17888685]

Yeh F-C, Panesar S, Fernandes D, Meola A, Yoshino M, Fernandez-Miranda JC, Vettel JM, Verstynen T, 2018. Population-averaged atlas of the macroscale human structural connectome and its network topology. Neuroimage 178, 57–68. [PubMed: 29758339]

Yeo BT, Sabuncu MR, Vercauteren T, Ayache N, Fischl B, Golland P, 2009. Spherical demons: fast diffeomorphic landmark-free surface registration. IEEE Trans Med Imaging 29 (3), 650–668. [PubMed: 19709963]

Zhang Q, Wang L, Zong X, Lin W, Li G, Shen D, 2019. Frnet: Flattened residual network for infant mri skull stripping. In: 2019 IEEE 16th International Symposium on Biomedical Imaging (ISBI 2019). IEEE, pp. 999–1002.

Zhang Y, Shi F, Wu G, Wang L, Yap P-T, Shen D, 2016. Consistent spatial-temporal longitudinal atlas construction for developing infant brains. IEEE Trans Med Imaging 35 (12), 2568–2577. [PubMed: 27392345]

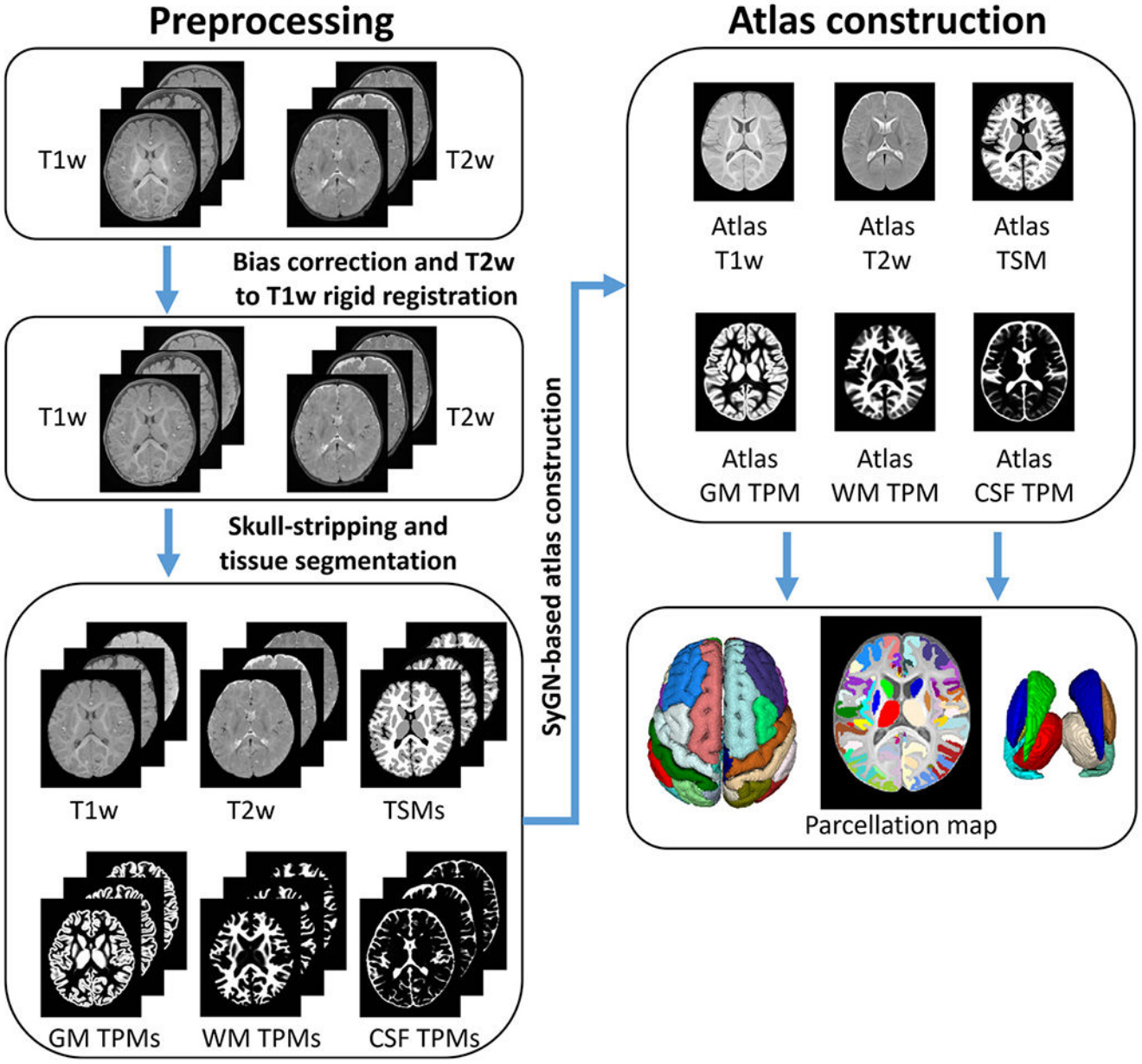

Fig. 1.
Flowchart for construction of infant brain volumetric atlas.

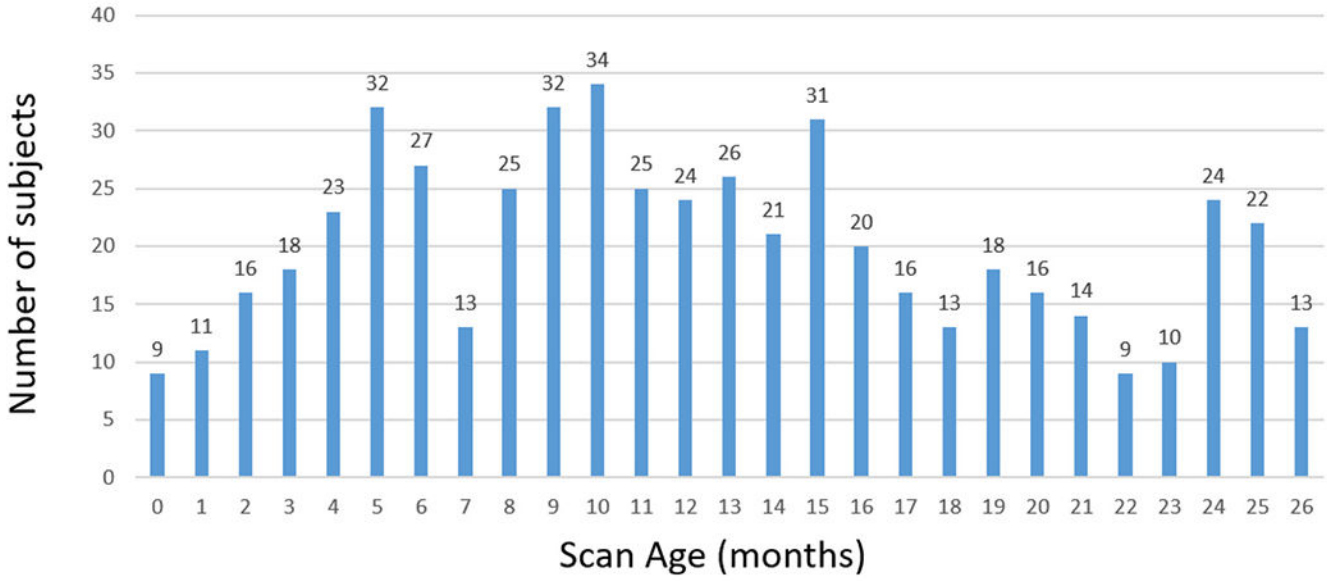

Fig. 2.
Number of subjects at each scan age.

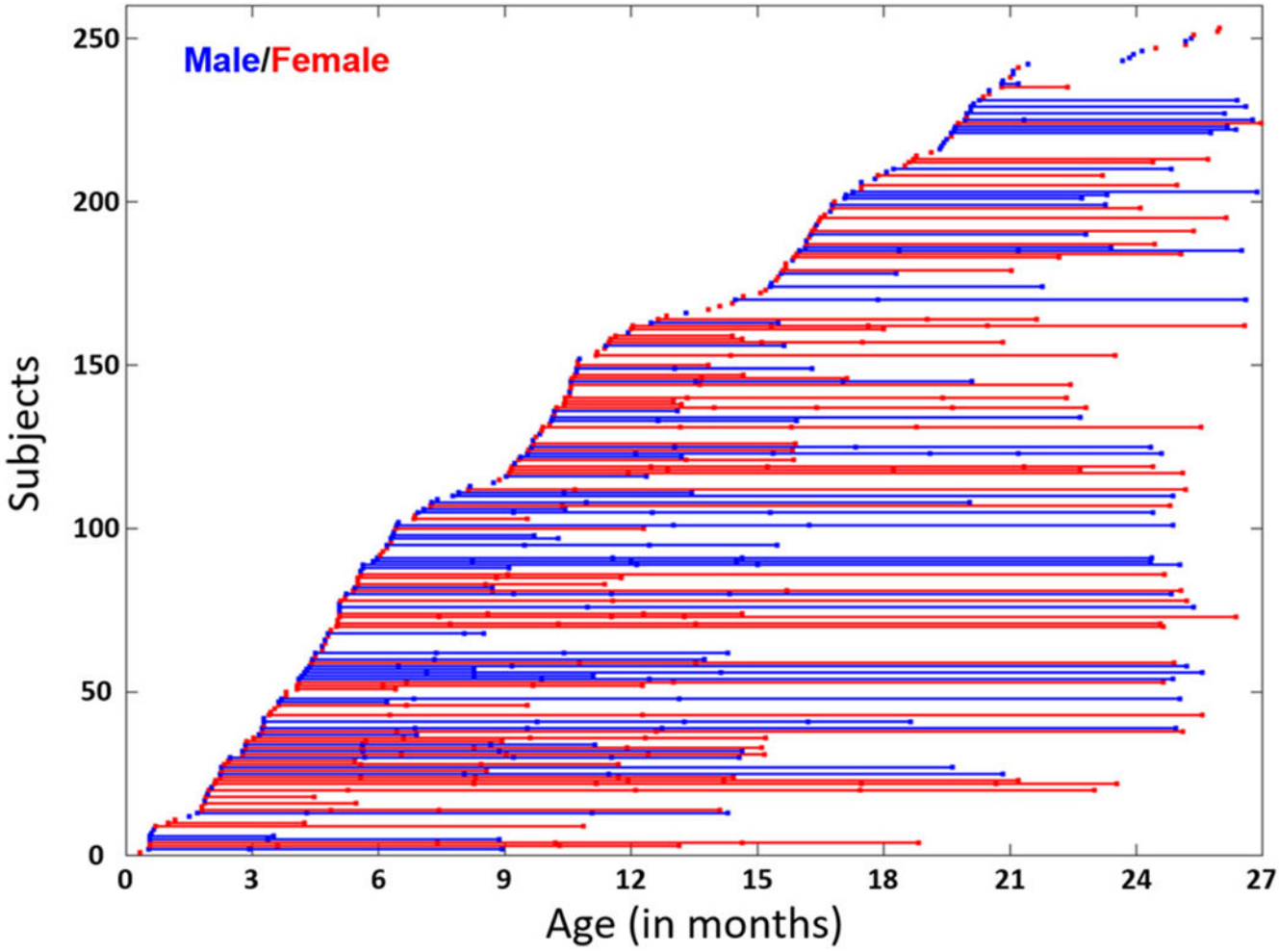

Fig. 3.

Longitudinal distribution of scans. Each line depicts one subject and each point exhibits one scan with the scan age shown on the x-axis.

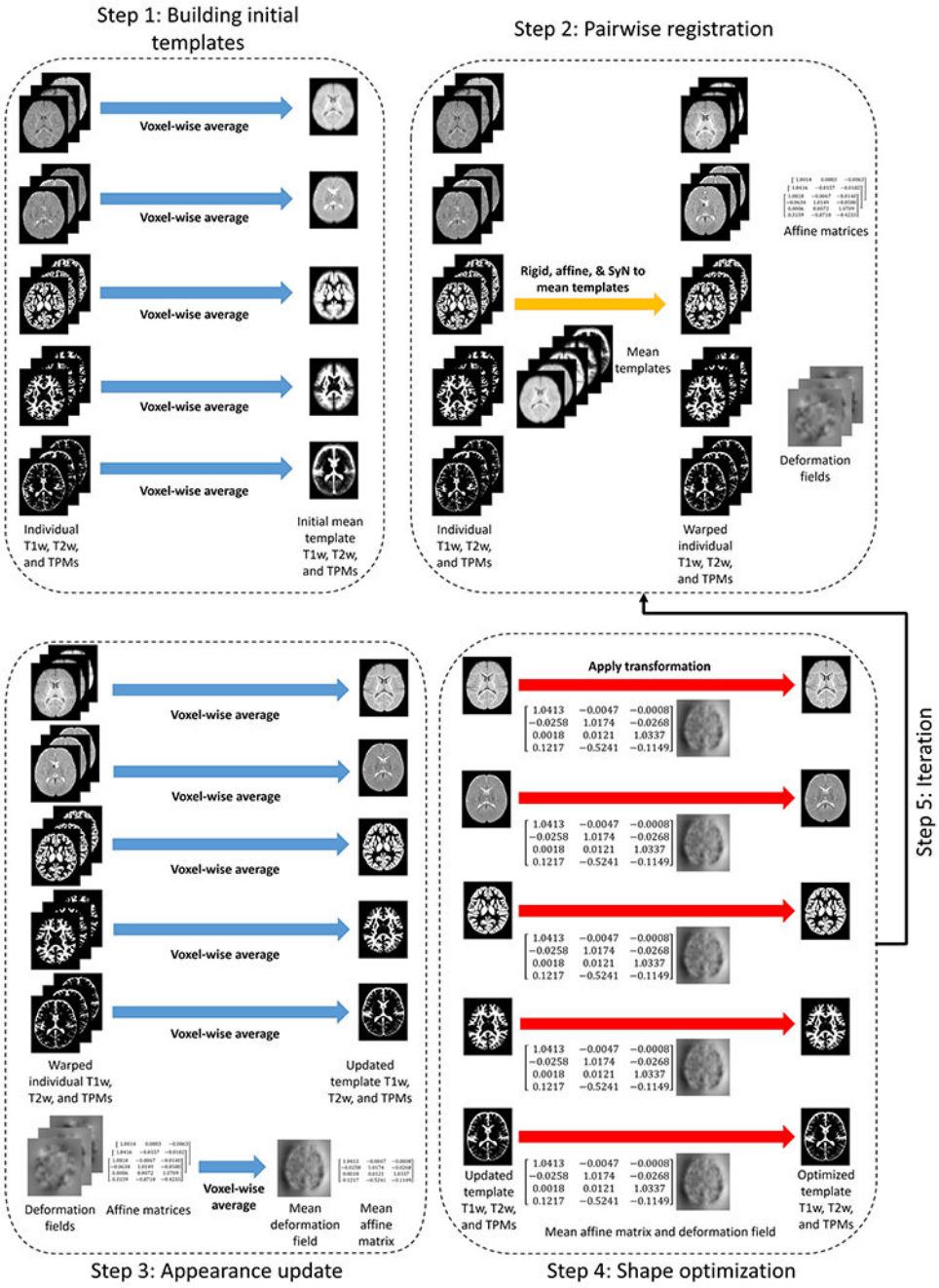

Fig. 4.
SyGN-based atlas construction.

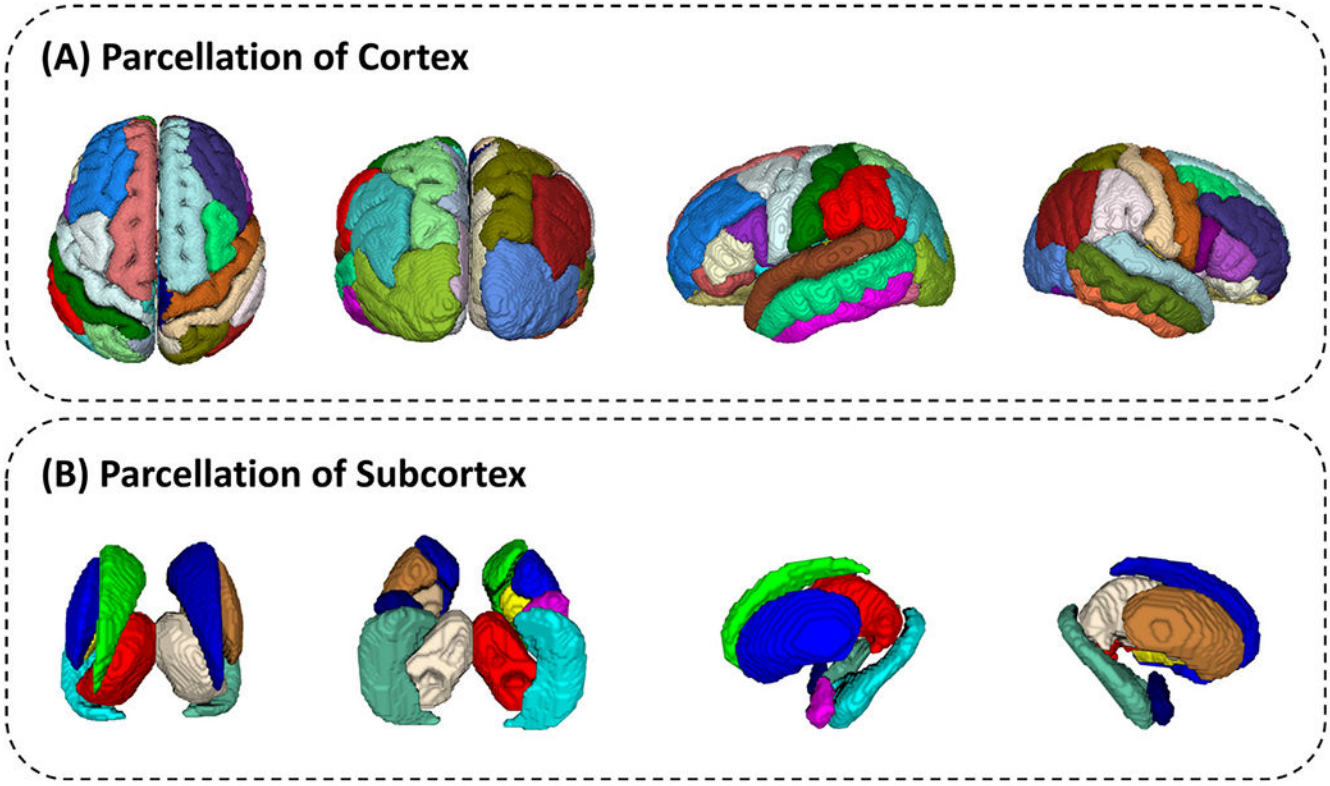

Fig. 5.

3D surface rendering of the generated parcellation maps. (A) Parcellation of cerebral cortex (35 cortical ROIs in each hemisphere); (B) parcellation of subcortex (6 subcortical ROIs in each hemisphere).

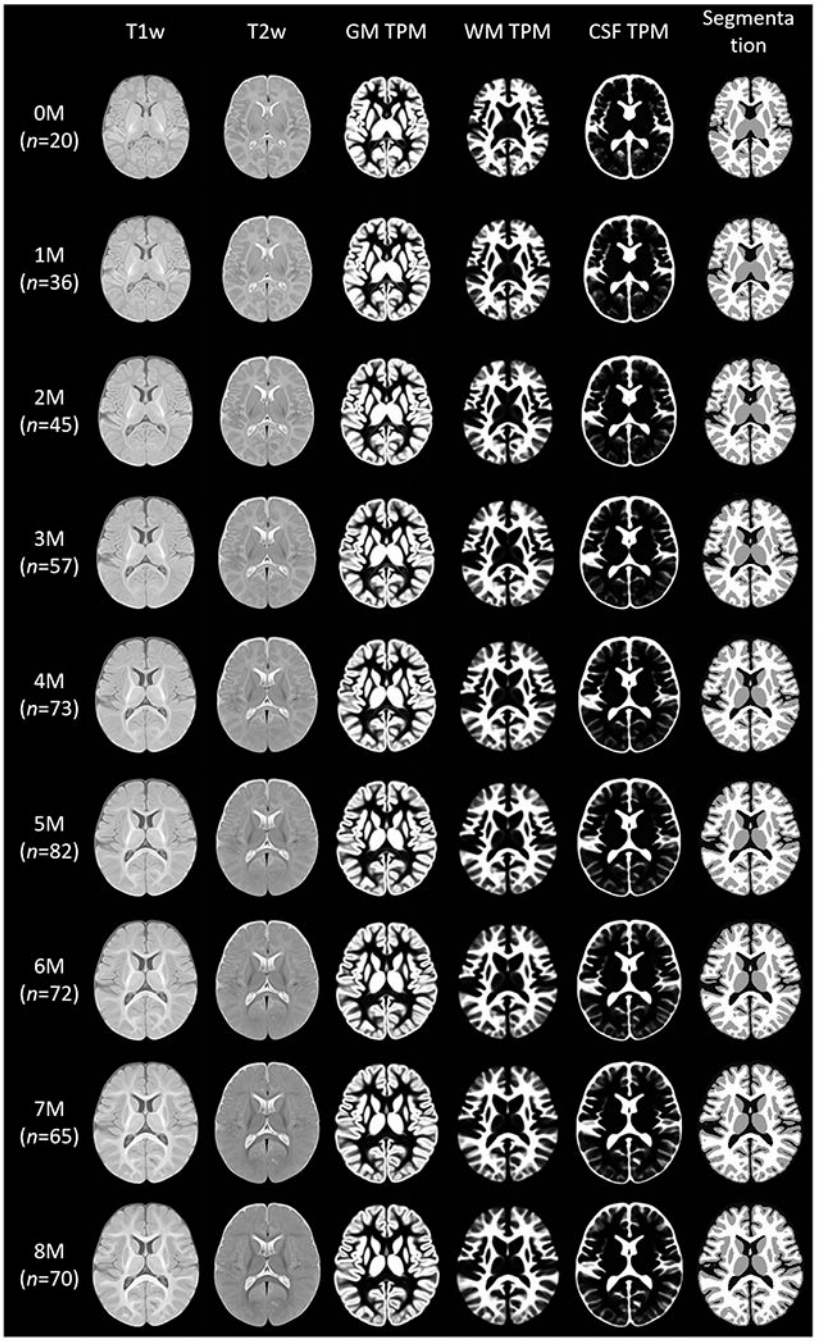

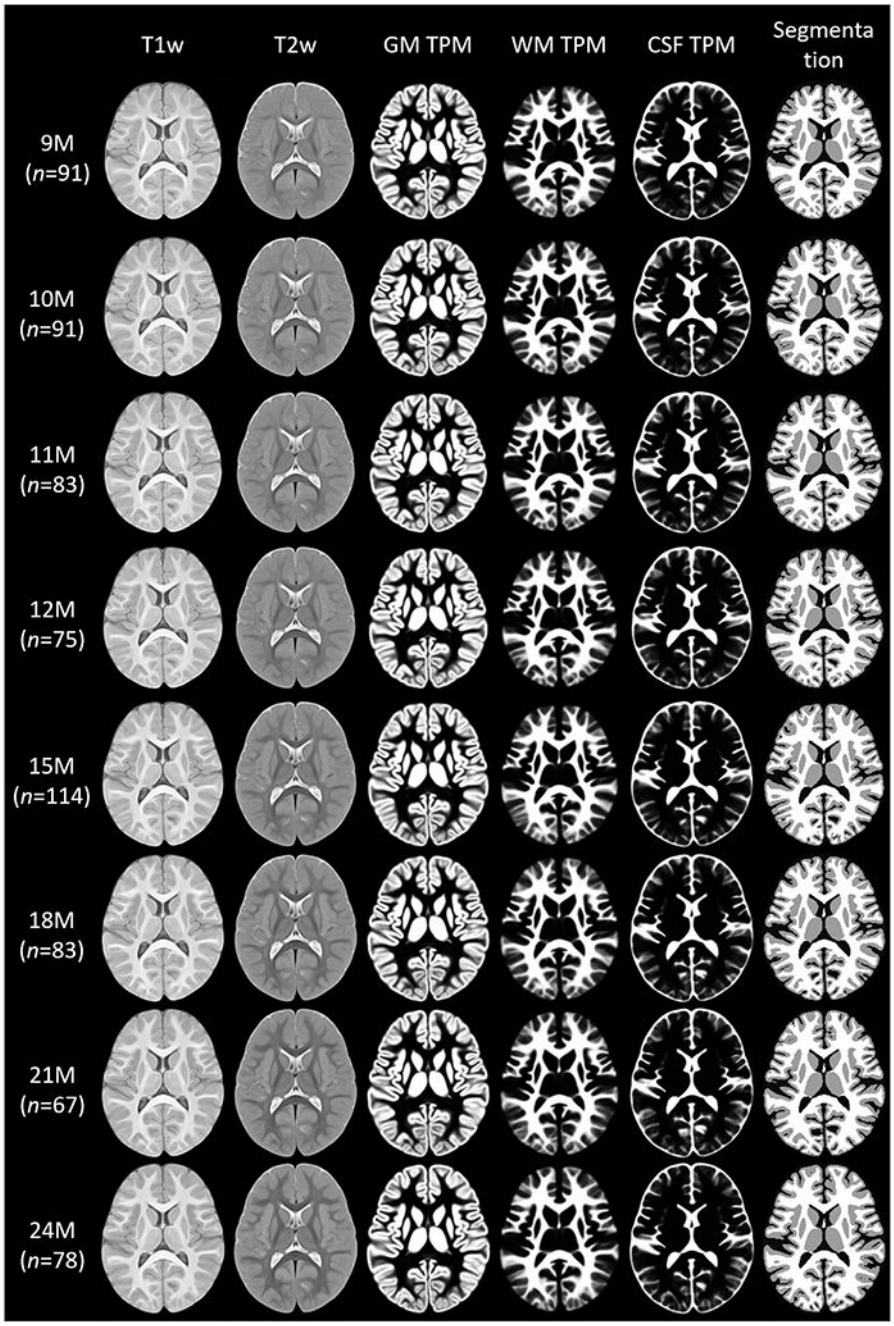

Fig. 6.
4D atlas from 0-month to 24-month.

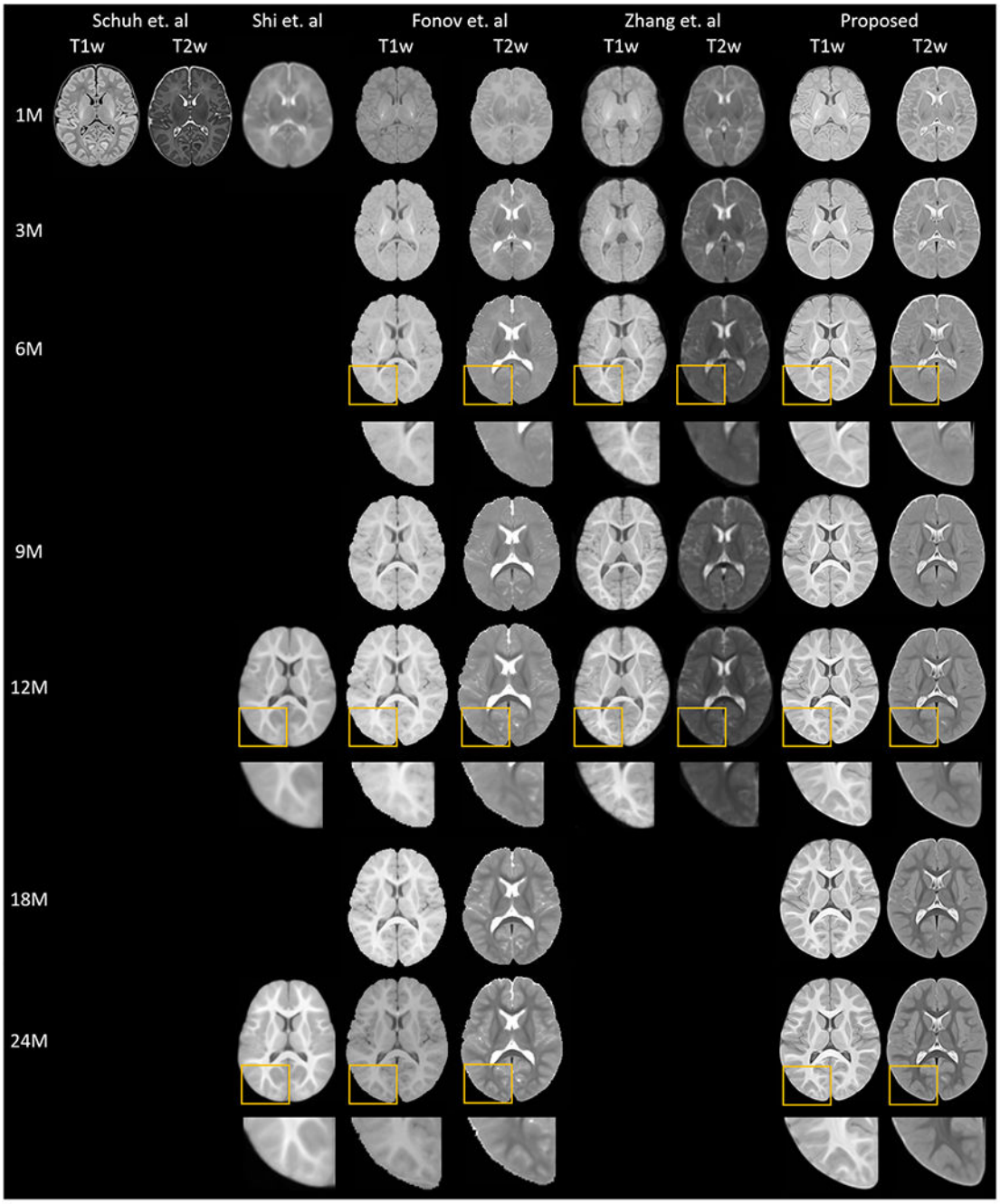

Fig. 7.
Visual comparison of existing atlases and the proposed 4D infant atlas.

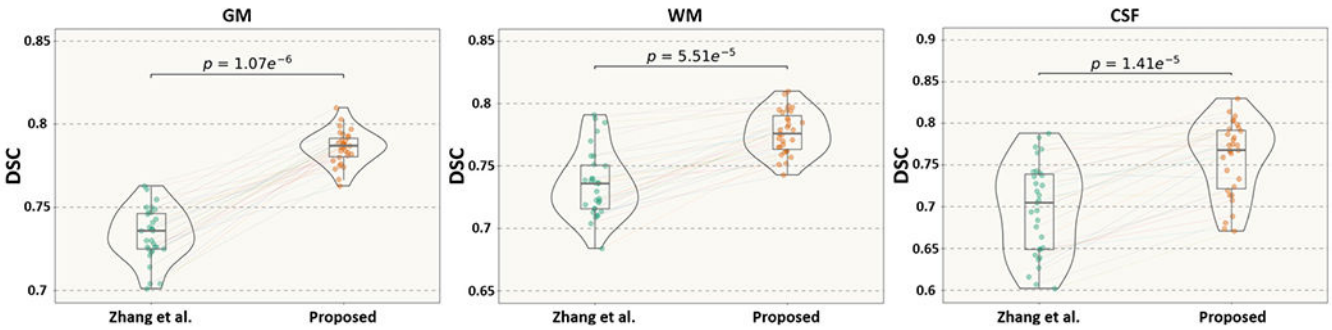

Fig. 8.

Quantitative evaluation results of the proposed atlas on the BCP datasets, compared to the atlas proposed by (Zhang et al., 2016), on the test images within the first year. Each point represents the Dice ratio value for one scan shown on the y-axis. We pair-wisely connected the Dice ratio values from the same scan based on different atlases for comparison.

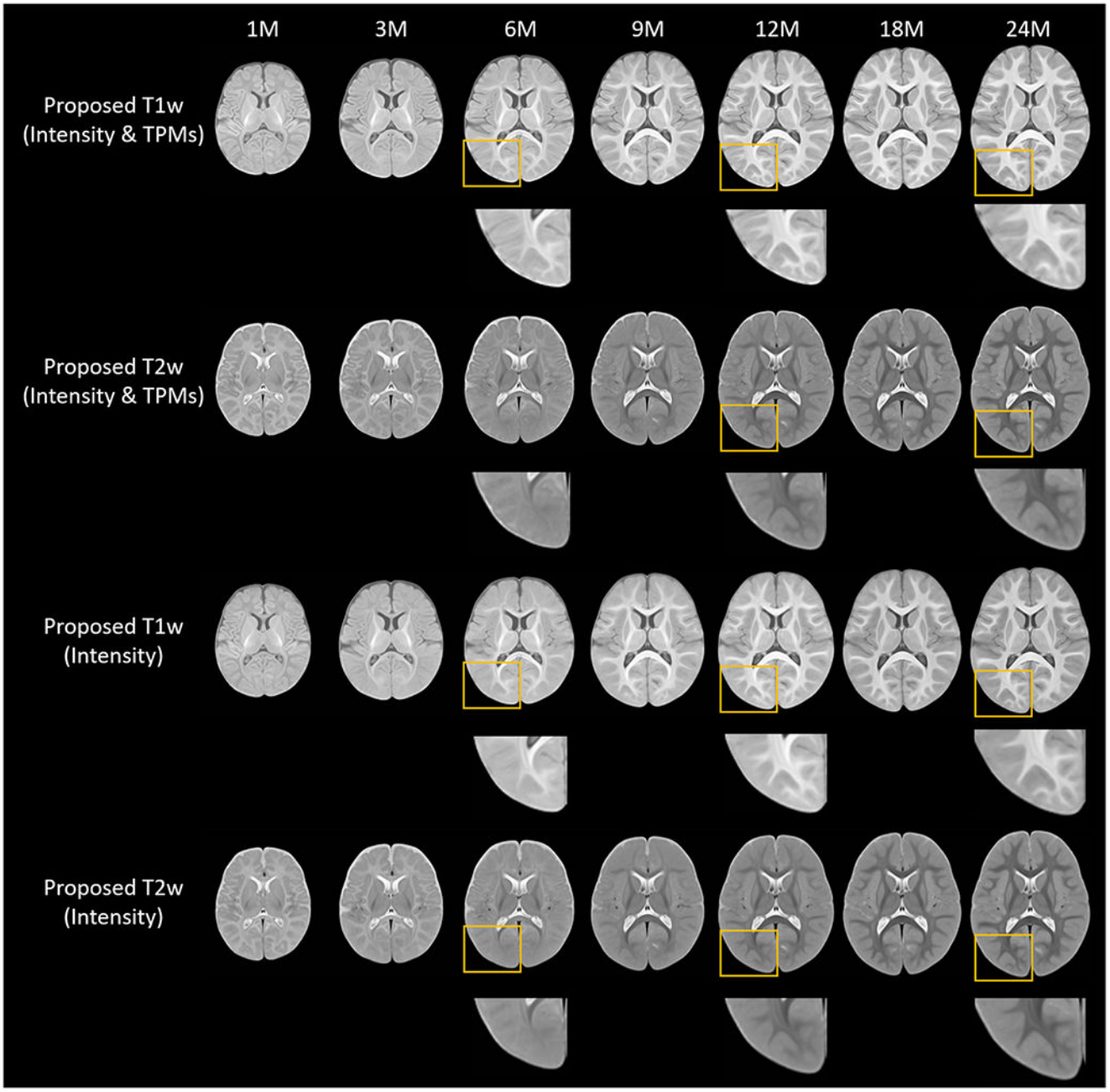

Fig. 9.
Visual comparison of the proposed atlases built w/o TPMs.

Table 1

Brief summary of recently published infant brain volumetric atlases.

Citation	Modalities	Age range	Subject number	Scan number	Resolution (mm^3)	Time points	Segmentation	Parcellation
Fonov et al. (2009)	T1w, T2w	0–54 months	108	317	1.0 × 1.0 × 1.0	9	No	No
Shi et al. (2011)	T1w, T2w	0–24 months	95	285	1.0 × 1.0 × 1.0	3	Yes	90 regions
Kuklisova et al. (2011)	T2w	Neonates GA 29–44 weeks	142	142	0.86 × 0.86 × 1.0	6	Yes	No
Oishi et al. (2011)	T1w, T2w	Neonates PMA 33–57 weeks	33	33	1.0 × 1.0 × 2.0	1	Yes	122 regions
Akiyama et al. (2013)	T1w	177–230 days	60	60	1.0 × 1.0 × 1.0	1	Yes	90 regions
Zhang et al. (2016)	T1w, T2w	0–12 months	35	150	1.0 × 1.0 × 1.0	5	Yes	No
Schuh et al. (2018)	T1w, T2w	Neonates PMA 33–44 weeks	275	275	0.5 × 0.5 × 0.5	9	Yes	87 regions
Proposed	T1w, T2w	0–24 months	240	542	0.8 × 0.8 × 0.8	17	Yes	82 regions

Table 2

The Dice ratios of the tissue segmentation based on different atlases.

Age (month)	Tissue	Schuh et al. (2018)	Shi et al. (2011)	Zhang et al. (2016)	Proposed
1M	GM	**78.3 ± 1.2**	72.9 ± 0.4	74.0 ± 1.5	77.8 ± 0.8
	WM	75.8 ± 2.5	71.1 ± 1.8	71.1 ± 2.6	**76.7 ± 1.8**
	CSF	63.5 ± 5.8	60.3 ± 3.2	76.5 ± 2.3	**78.8 ± 1.7**
3M	GM	N/A	N/A	74.7 ± 0.7	**78.1 ± 0.7**
	WM	N/A	N/A	78.1 ± 1.0	**80.2 ± 0.7**
	CSF	N/A	N/A	76.0 ± 2.4	**80.6 ± 2.7**
6M	GM	N/A	N/A	71.4 ± 1.4	**77.1 ± 1.0**
	WM	N/A	N/A	72.2 ± 1.8	**75.9 ± 1.9**
	CSF	N/A	N/A	68.5 ± 4.3	**76.5 ± 3.6**
9M	GM	N/A	N/A	72.9 ± 0.9	**78.8 ± 0.6**
	WM	N/A	N/A	72.2 ± 1.5	**77.6 ± 1.7**
	CSF	N/A	N/A	63.2 ± 3.2	**71.4 ± 3.4**
12M	GM	N/A	73.9 ± 0.7	74.2 ± 0.6	**79.4 ± 0.9**
	WM	N/A	73.3 ± 1.4	74.7 ± 1.1	**78.1 ± 1.7**
	CSF	N/A	72.4 ± 2.0	71.8 ± 2.3	**75.2 ± 4.0**
24M	GM	N/A	78.8 ± 0.7	N/A	**82.1 ± 0.8**
	WM	N/A	76.1 ± 1.0	N/A	**80.3 ± 1.5**
	CSF	N/A	76.2 ± 1.5	N/A	**79.5 ± 3.2**

Table 3

The Dice ratios of the tissue segmentation based on the proposed atlases built w/o TPMs.

	Tissue	1M	3M	6M	9M	12M	18M	24M
Proposed	GM	77.8 ± 0.8	78.1 ± 0.7	77.1 ± 1.0	78.8 ± 0.6	79.4 ± 0.9	79.5 ± 1.3	82.1 ± 0.8
	WM	76.7 ± 1.8	80.2 ± 0.7	75.9 ± 1.9	77.6 ± 1.7	78.1 ± 1.7	78.9 ± 2.3	80.3 ± 1.5
	CSF	78.8 ± 1.7	80.6 ± 2.7	76.5 ± 3.6	71.4 ± 3.4	75.2 ± 4.0	79.3 ± 2.7	79.5 ± 3.2
Proposed (Intensity)	GM	77.5 ± 1.1	76.2 ± 0.8	75.4 ± 1.2	77.4 ± 1.1	77.3 ± 1.5	77.9 ± 1.8	81.7 ± 0.6
	WM	76.1 ± 2.2	79.6 ± 1.1	75.1 ± 2.1	76.5 ± 1.3	77.1 ± 1.8	76.4 ± 2.4	79.2 ± 1.4
	CSF	78.6 ± 1.9	78.9 ± 2.9	75.1 ± 3.4	70.6 ± 2.8	78.8 ± 3.7	78.5 ± 2.8	78.4 ± 3.0

Table 4

The Dice ratios of the warped tissue segmentation maps on the NDAR dataset.

Age (month)	Tissue	Shi et al. (2011)	Zhang et al. (2016)	Proposed
6M	GM	N/A	59.5 ± 1.8	**63.1 ± 1.0**
	WM	N/A	66.4 ± 2.3	**70.2 ± 0.9**
	CSF	N/A	57.3 ± 2.7	**61.0 ± 1.4**
12M	GM	67.3 ± 0.7	67.7 ± 0.8	**69.0 ± 0.7**
	WM	69.4 ± 1.3	68.7 ± 0.9	**71.1 ± 0.7**
	CSF	56.9 ± 1.8	57.7 ± 1.9	**58.7 ± 1.7**
24M	GM	71.4 ± 0.7	N/A	**73.2 ± 0.7**
	WM	71.5 ± 0.8	N/A	**73.4 ± 0.8**
	CSF	53.7 ± 1.6	N/A	**55.3 ± 1.5**